A DEM-FEM exploratory study on the mechanical interaction between lipid particles and the endothelial glycocalyx layer

Ricardo A. Andreotti[1], Eduardo M. B. Campello[1]

[1]*Dept. of Structural and Geotechnical Engineering, Polytechnic School, University of São Paulo*
Av. Prof. Almeida Prado, 05508-900, São Paulo, Brazil
ricardo.andreotti@usp.br, campello@usp.br

Abstract. This work develops an exploratory study aiming at modeling (from a purely mechanistic point of view) the complex interactions that are observed between the Endothelial Glycocalyx Layer (EGL) and Low-Density Lipoprotein (LDL) particles, serving as a gateway to more complex studies about the transport of macromolecules in arterial vessels. Here, the EGL is represented through an advanced finite element formulation for thin, large-deformation beams, following a continuum description. The LDL particles, in turn, are handled through a discrete element approach. The two phases (discrete and continuum) interact with each other through multiple contacts and collisions, the forces and moments of which being thoroughly computed and passed from a discrete element (DEM) to the finite element (FEM) model (and vice-versa) at run-time in a staggered, iterative solution scheme, following the framework developed by the authors in Gay Neto and Campello [1] and Andreotti et al. [2]. The fluid (blood) phase is represented only indirectly, through drag forces applied on both the FEM beams and DEM particles. Possibilities of the proposed strategy are illustrated through a preliminary numerical example, herein taken in the form of a model problem.

Keywords: Endothelial Glycocalyx Layer, Low-Density Lipoprotein Particles, Finite Element Method, Discrete Element Method.

1 Introduction

Atherosclerosis consists of the accumulation of atherogenic lipids such as low-density lipoproteins (LDLs) within arterial walls (Liu et al. [3]). There have been many studies in the area trying to unfold the transport of macromolecules within the arterial wall through both experiments and computational simulations (Karner et al. [4], Ai and Vafai [5], Saidel et al. [6]). However, most of them ignored the Endothelial Glycocalyx Layer (EGL), which functions as an inhibitor of the diffusion of LDL near the luminal surface of the endothelium (Vincent et al. [7]). The EGL is a thin (circa 500 nm height), fur-like, protein-lipid layer that coats the membrane of some types of cells and, in particular, the luminal surface of blood vessels (Pries et al. [8]). Its main roles are to act as a modulator of permeability in the transcapillary exchange of water, as a mechanotransducer of fluid shear stress to the endothelial cytoskeleton, and as a regulator of red and white blood cells interactions, with emphasis on the inflammatory response. For blood flows, it is known that the mechanical properties of the EGL may strongly influence its interaction with passing red and white blood cells (Weinbaum et al. [9]), as well as with small suspended lipid (especially LDL) particles. This includes its deformation owing to blood fuid-dynamic loads, as well as contact interactions with the passing cells and lipid particles. From a mechanistic point of view, the EGL resembles thin, highly deformable fur threads fixed at the base at rather patterned points of the vessel's interior walls, with elastic properties that are fairly well known.

To understand the role of the EGL as a physical barrier, in this work we develop an exploratory study aiming at modeling (from a purely mechanistic point of view) the complex interactions that are observed between the EGL and LDL particles, serving as a gateway to more complex studies about the transport of macromolecules in the arterial vessels. The EGL is represented through an advanced finite element (FEM) formulation for thin, large-deformation beams, following a continuum description. The LDL particles, in turn, are handled through a discrete

element (DEM) approach. We use elastic properties established in the literature, and analyze the mechanical behavior of the EGL's structure when it comes into contact with passing LDL particles. The fluid (blood) phase is represented only indirectly, through drag forces applied on both the FEM beams and DEM particles. Throughout the text, italic letters ($a, b, \ldots \alpha, \beta, \ldots A, B, \ldots$) denote scalar quantities, boldface italic small-cap letters ($\boldsymbol{a}, \boldsymbol{b}, \ldots \boldsymbol{\alpha}, \boldsymbol{\beta}, \ldots$) denote vectors and boldface italic capital letters ($\boldsymbol{A}, \boldsymbol{B}, \ldots$) denote second-order tensor in a three-dimensional Euclidian space.

2 Description of the EGL structure and properties

According to Weinbaum et al. [9], computer-enhanced images showed that the EGL is a three-dimensional fibrous network consisted of fur-like threads of circa 10–12-nm-diameter, with focal scattering centers spaced of 20 nm in all directions, and a length varying from 150 to 400 nm, forming a "bush" structure in an hexagonal array (when seen from the top) with a spacing of 100 nm (center to center), as schematically represented in Fig. 1.

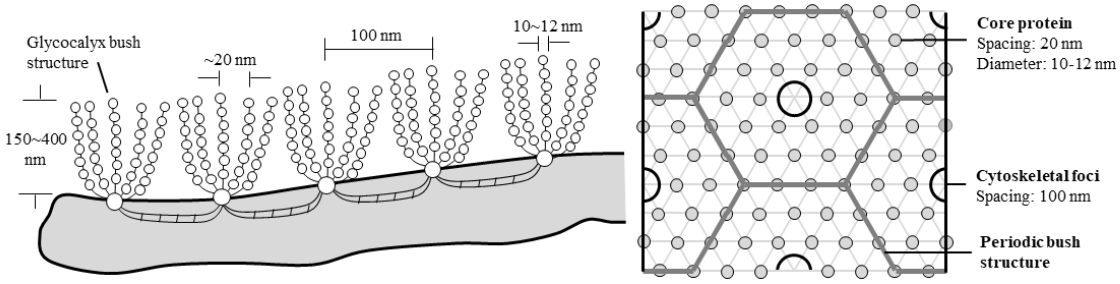

Figure 1. Schematic representation of the EGL. The left figure shows the view of core proteins (fur-like threads) and its anchorage to the underlying actin cortical cytoskeleton. The right figure represents the top view of the hexagonal arrangement and its cluster foci. Adapted from Weinbaum et al. [9].

One important parameter for defining the deformation of the EGL (and thereby to our mechanical analysis) is its flexural rigidity EI (where E is the elastic modulus and I the bending inertia). However, there is no direct measurement of it. Han et al. [10] developed a sophisticated large deformation model, predicting the time-dependent change in the shape of the core proteins after the passage of a white blood cell, arriving at an EI of 490 pN nm^2. We will use this value here.

3 Description o f the idealized model

To construct our mechanical model to assess the behavior of the EGL interacting with lipid particles, we will first summarize our kinematical model for large-deformation beams. The EGL bush-like structure will be represented as a set of highly deformable beams (the fur-like threads) fixed at the base, following an advanced finite element formulation. Then, we will summarize the description of the the LDL particles through a discrete element approach, whereby we map the motion of each individual particle. Lastly, as the two phases (discrete and continuum) may interact with each other through multiple contacts and collisions, we will summarize our interaction framework, as developed by the authors in Gay Neto and Campello [1] and Andreotti et al. [2].

3.1 Summary of the FEM model

Let us consider a beam with reference length l and local unitary orthogonal system $\{\boldsymbol{e}_1^r, \boldsymbol{e}_2^r, \boldsymbol{e}_3^r\}$, with corresponding coordinates $\{\xi_1^r, \xi_2^r, \xi_3^r\}$. We follow the geometrically-exact quasi-static model of Pimenta and Yojo [11] and Pimenta, Campello and Wriggers [12], which will be discretized and solved by the finite element method. Accordingy, each cross-section remains undeformed in time and may only displace and rotate as a rigid body. The position of the beam´s material points, in the reference configuration, is represented by vector $\boldsymbol{\xi}$, as seen in Fig. 2-a, which is written as

$$\boldsymbol{\xi} = \boldsymbol{\zeta} + \boldsymbol{a}^r, \tag{1}$$

where $\boldsymbol{\zeta} = \zeta \boldsymbol{e}_3^r$ is the position of points along the beam axis (with $\zeta = [0, l]$) and $\boldsymbol{a}^r = \xi_1 \boldsymbol{e}_1^r + \xi_1 \boldsymbol{e}_1^r$ is the reference director, which gives the relative position of points of the cross-section w.r.t. the beam axis. In the current configuration, we define a local orthogonal system $\{\boldsymbol{e}_1, \boldsymbol{e}_2, \boldsymbol{e}_3\}$ with corresponding coordinates ξ_1, ξ_2, ξ_3, with which the motion is described by the vector field $\boldsymbol{x} = \widetilde{\boldsymbol{x}}(\boldsymbol{\xi})$, with the material points positions given by

$$\boldsymbol{x} = \boldsymbol{z} + \boldsymbol{a}, \tag{2}$$

with $\boldsymbol{z} = \boldsymbol{\zeta} + \boldsymbol{u}$ describing the position of points in the deformed beam axis, $\boldsymbol{u}$ the displacement vector and $\boldsymbol{a} = \boldsymbol{Q}\boldsymbol{a}^r$ the current director at those points. The rotational field is parameterized using the so-called Rodrigues rotation vector $\boldsymbol{\alpha} = \alpha \boldsymbol{e}$, with $\alpha = 2\tan(\theta/2)$, in which $\boldsymbol{\theta} = \theta \boldsymbol{e}$ is the classical Euler rotation vector, with θ the magnitude of the rotation and $\boldsymbol{e}$ the unit rotation axis. Thus, the rotation tensor $\boldsymbol{Q}$ reads as

$$\boldsymbol{Q} = \boldsymbol{I} + \frac{4}{1+\alpha^2}\left[\boldsymbol{A} + \frac{1}{2}\boldsymbol{A}\right], \tag{3}$$

with $\boldsymbol{A} = \text{Skew}(\boldsymbol{\alpha})$. Derivation of (2) w.r.t. $\boldsymbol{\xi}$ renders the deformation gradient, from which the model´s strains follow. The stresses, in turn, are described by the first Piola-Kirchhoff stress tensor, with which we compute the cross-sectional stress resultants (forces and moments) and therefrom apply the virtual work theorem as to build the model´s weak form. We will not report their expressions here for conciseness (the interested reader is referred to the above-mentioned references). Finite element discretization of the weak form (with the axis´ displacements and rotations as unknowns) is performed in a standard way, using 3-node elements with quadratic shape-functions. For time integration of the beam´s dynamics, we adopt a implicit Newmark algorithm (see, e.g., Wriggers [13]).

3.2 Summary of the DEM model

The motion of the discrete solid particles follows a Lagrangian description here. We assume the particles are spherical. Any deformation they experience is presumed to be very small and localized, therefore they can be treated as rigid bodies. The model herein summarized is described in depth in Campello [14, 15]. Let us consider a system of N_P particles, each one with mass m_i, radius r_i and rotation inertia $j_i = 2/5\,(m_i r_i^2)$, with $i = 1, \ldots, N_P$. The position of a particle will be denoted by vector $\boldsymbol{x}_i$, its velocity by $\boldsymbol{v}_i$ and its spin by $\boldsymbol{w}_i$. The rotation vector relative to the beginning of the motion is denoted by $\boldsymbol{\alpha}_i$, whereas the incremental rotation vector is denoted by $\boldsymbol{\alpha}_i^{\Delta}$. The rotation field here is also parameterized using the Rodrigues rotation vector (see Eq. (3)), instead of the classical Euler rotation vector. For a detailed account of the rotation description, we refer the reader to Campello [16].

From Euler's laws, the following equations must hold for each particle at every time instant t,

$$m_i \ddot{\boldsymbol{x}}_i = \boldsymbol{f}_i^{\text{tot}} \quad \text{and} \quad j_i \dot{\boldsymbol{w}}_i = \boldsymbol{m}_i^{\text{tot}}, \tag{4}$$

in which $\boldsymbol{f}_i^{\text{tot}}$ is the total force vector acting on the particle and $\boldsymbol{m}_i^{\text{tot}}$ the total moment vector concerning the particle's center. The superposed dots denote time differentiation. The total force $\boldsymbol{f}_i^{\text{tot}}$ is the sum of the following force contributions

$$\boldsymbol{f}_i^{\text{tot}} = m_i \boldsymbol{g} + \boldsymbol{f}_i^{\text{drag}} + \boldsymbol{f}_i^{\text{nf}} + \boldsymbol{f}_i^{\text{con,p}} + \boldsymbol{f}_i^{\text{fric,p}} + \boldsymbol{f}_i^{\text{con,beam}}, \tag{5}$$

where $\boldsymbol{g}$ is the gravity acceleration vector, $\boldsymbol{f}_i^{\text{drag}}$ is the drag force vector, $\boldsymbol{f}_i^{\text{nf}}$ are the forces due to the near-field interactions with others particles, $\boldsymbol{f}_i^{\text{con,p}}$ are the normal forces due to contacts stemming from collisions with other particles as well as obstacles and rigid walls (herein given through Hertz contact theory), $\boldsymbol{f}_i^{\text{fric,p}}$ are the tangential forces due to friction caused by these collisions (herein given through a consistent stick-slip scheme) and $\boldsymbol{f}_i^{\text{con,beam}}$ the forces due to contacts with FEM beams (which include both normal and frictional contributions, coming from solution of the particle-beam contact problem as described in section 3.3). In the same way, the total moment applied on the particle is given by the sum of the following contributions:

$$\boldsymbol{m}_i^{\text{tot}} = \boldsymbol{m}_i^{\text{fric,p}} + \boldsymbol{m}_i^{\text{con,beam}} \tag{6}$$

where $\boldsymbol{m}_i^{\text{fric,p}}$ is the moment generated by the friction forces from other particles (and obstacles and rigid walls)

and $\boldsymbol{m}_i^{\text{con,beam}}$ is the moment generated by the friction forces from neighboring beams. Detailed expressions for these force and moment contributions will not be reported here for conciseness (see Campello [14]). Numerical time integration of Eq. (4) provides the particles' motion. This is done here through the integration algorithm proposed in Campello [14], which has both implicit and explicit versions. In this work, we adopt the explicit version only, since the inter-particle contacts inherently require very small time-steps for an accurate contact representation, thus rendering the implicit version unnecessary. The integration algorithm will be omitted here.

3.3 Particle-beam and beam-beam contact scheme

The interaction between particles and beams follows a simple strategy, which has been successfully proposed by the authors in Gay Neto and Campello [1]. In this approach, the beam is assumed to have a circular cross-section, and for contact detection purposes it is treated as a set of fictitious spheres (with the same radius of the beams' cross-section) whose centers lie on the nodes of the beam's FEM mesh (see Fig 2b). We emphasize that this is for the sake of contact detection only, not for its kinematics. The reason is the simplicity of such contact topology (which amounts to a sphere-sphere contact), becoming one of the advantages of this approach because it spares the solution to a minimum distance problem, which could be untenable for large multi-particle, multi-beam systems. We note that the level of refinement of the beam's finite element mesh is dictated by the number of fictitious spheres that is desired for contact detection - the more refined, the more accurate the contact resolution.

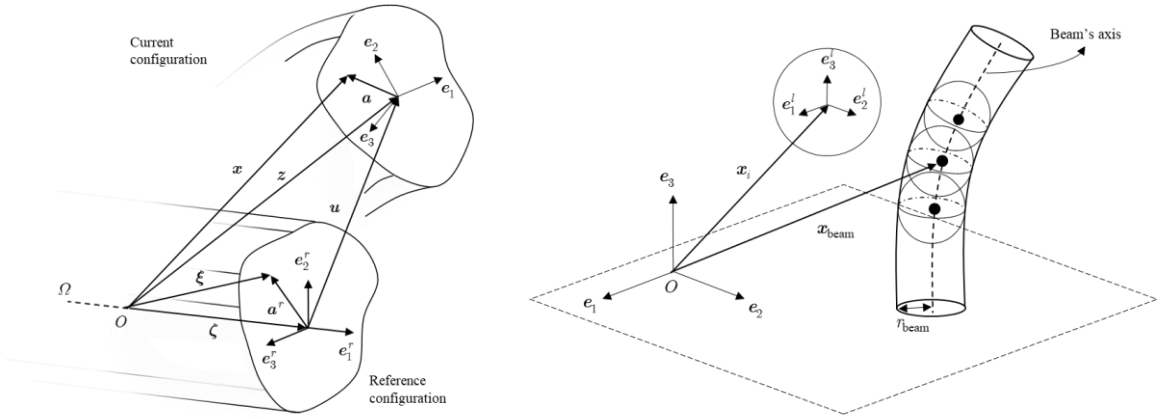

Figure 2. The left figure describes the beam's geometry and basic kinematical quantities. The right figure presents the imminent contact between a particle and a fictitiuous sphere of a beam.

As contact occurs, the normal gap g_n of the contact pair is defined as a function of the spheres' centers positions, i.e.,

$$\mathrm{g}_n = \left\| \boldsymbol{x}_{beam} - \boldsymbol{x}_i \right\| - r_{beam} + r_i \tag{7}$$

in which $\boldsymbol{x}_{beam}$ is the beam's sphere position (which coincides with the position of a node of the underlying FEM mesh) on the current configuration and r_{beam} its cross-section radius (see Fig. 2b). The contact pair will add a contribution W_n to the potential energy of the beam, and this is done here through the penalty method, with a normal penalty parameter ε_n such that $W_n = 1/2(\varepsilon_n \mathrm{g}_n^2)$. The corresponding contribution on the beam´s weak form is $\delta W_n = \varepsilon_n \mathrm{g}_n \cdot \delta \mathrm{g}_n$, with $\delta \mathrm{g}_n = \boldsymbol{n} \cdot \ \delta \boldsymbol{x}_{beam} - \delta \boldsymbol{x}_i$, where $\boldsymbol{n}$ is the contact normal vector as follows

$$\boldsymbol{n} = \frac{\boldsymbol{x}_{beam} - \boldsymbol{x}_i}{\left\| \boldsymbol{x}_{beam} - \boldsymbol{x}_i \right\|}. \tag{8}$$

The contact will generate a force $\boldsymbol{f}_i^{\text{con,beam}} = -\varepsilon_n \mathrm{g}_n \boldsymbol{n}$ on the particle, which will be summed up on the particle's total force vector $\boldsymbol{f}_i^{\text{tot}}$, as seen in Eq. (5). The tangential (friction) contribution is handled through a stick-slip scheme (not reported here for conciseness). For beam-beam interactions, in turn, we follow the strategy

proposed in Gay Neto, Pimenta, and Wriggers [17], which also resorts to the concept of fictitious spheres for dectection purposes, along with a penalty formulation similar to the one described above. The scheme will be omitted here.

The models were implemented in our in-house codes PSY and GIRAFFE, in which PSY [18] (written in Fortran) handles the DEM analysis of the particles, whereas GIRAFFE [19] (written in C++) handles the FEM and contact analyses of the beams. The two codes were coupled in an efficient manner, making use of the C/C++ and Fortran interoperability capacity, enabling full run-time, memory-sharing communication between the codes. This unified project was called GIPSY, and further details are described in Andreotti et al. [2].

4 Preliminary results

In this section we present some preliminary results obtained with a simple numerical example. Accordingly, the bush-like EGL structure is represented by a set of beams (36 in total for each "bush") following the arrangement seen in Fig. 1. We consider here seven of such bushes. Each beam is discretized with twenty 3 three-node finite elements. To simplify matters, since the EGL diameter varies between 10~12 nm over each filament, the beams were considered with fixed diameters of 10 nm, and their length set to 300 nm. Consequently, the bending inertia I is 4.909×10^{-34} m^4, and since $EI = 4.9 \times 10^{-28}$ Nm^2, an elastic modulus of $E = 0.998$ MPa follows. The mass density considered for the EGL is $\rho_{EGL} = 1053$ kg/m^3. As the action of gravity is negligible in such small scales, it is not considered here.

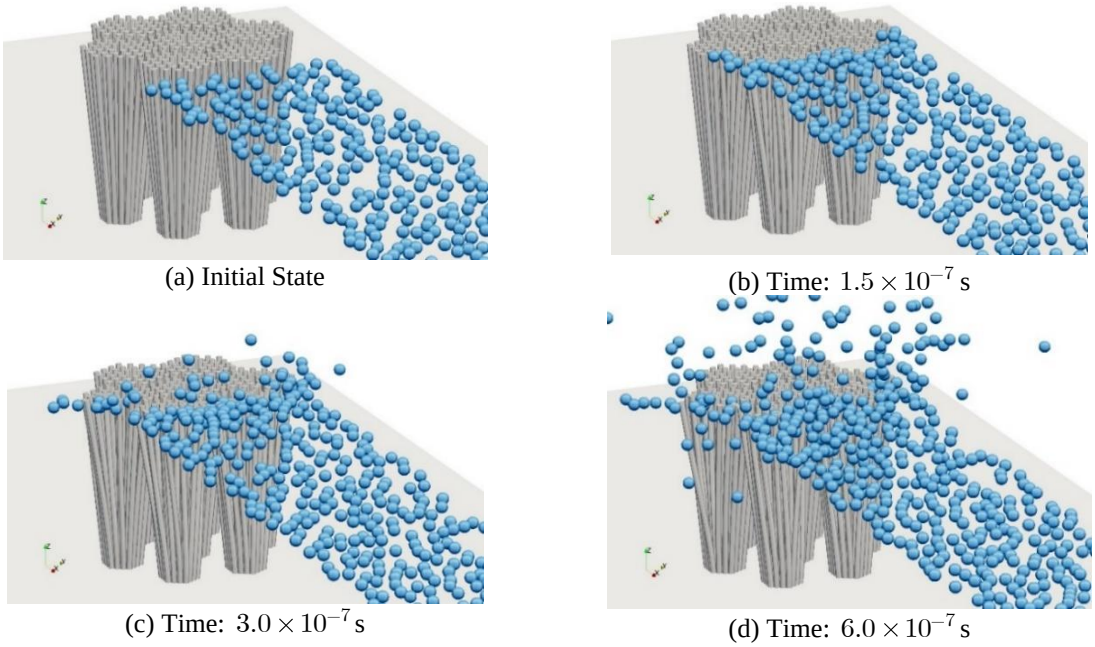

(a) Initial State

(b) Time: 1.5×10^{-7} s

(c) Time: 3.0×10^{-7} s

(d) Time: 6.0×10^{-7} s

Figure 3. Snapshots of the motion at some selected time instants.

The LDL particles' diameters vary among humans, and their size is intrinsically related to the total and cardiovascular mortality (Grammer et al. [20]). For that matter, we estimated a range of 20-30 nm for the particle diameter, with an elastic modulus of 1.5 MPa (which is inside the range of 0.1~2.5 MPa, defined by Takeda et al. [21]).

The particles and the beams are assumed to be immersed in an arterial vessel, inside of which we assume that the blood flows at a constant velocity of $\{1.3; 0.0; 0.0\}$ m/s (this value is taken from Klarhöfer et al. [22], which defines some average blood flows in arterial and venous blood vessels). The blood has a mass density of $\rho_{bl} = 1060$ kg/m³ (Kenner [23]) and an average viscosity of 3.5×10^{-3} Pa $\cdot$ s (Nader et al. [24]). The penalty parameter for the beam-particle (and for the beam-beam) contact is $\varepsilon_n = 1.488 \times 10^{-3}$ N/m. The endothelial surface is assumed flat and rigid. The time step adopted is $\Delta t = 1 \times 10^{-10}$ s (for both DEM and FEM solutions),

with a simulation time of $t = 6.0 \times 10^{-7}$ s. The convergence tolerance within the Newton iterations is $tol = 10^{-8}$, for unbalanced forces, moments, incremental displacements and rotations. No tolerance was needed on the DEM solver since we are using the explicit version of the method.

We also include structural damping (i.e., damping on the beam's deformation), assuming a Rayleigh type damping, with $\alpha = 0$ and $\beta = 1 \times 10^{-5}$. Inasmuch, the normal damping parameter for particles is defined by $\xi^{con} = 0.15$ (Campello [14]).

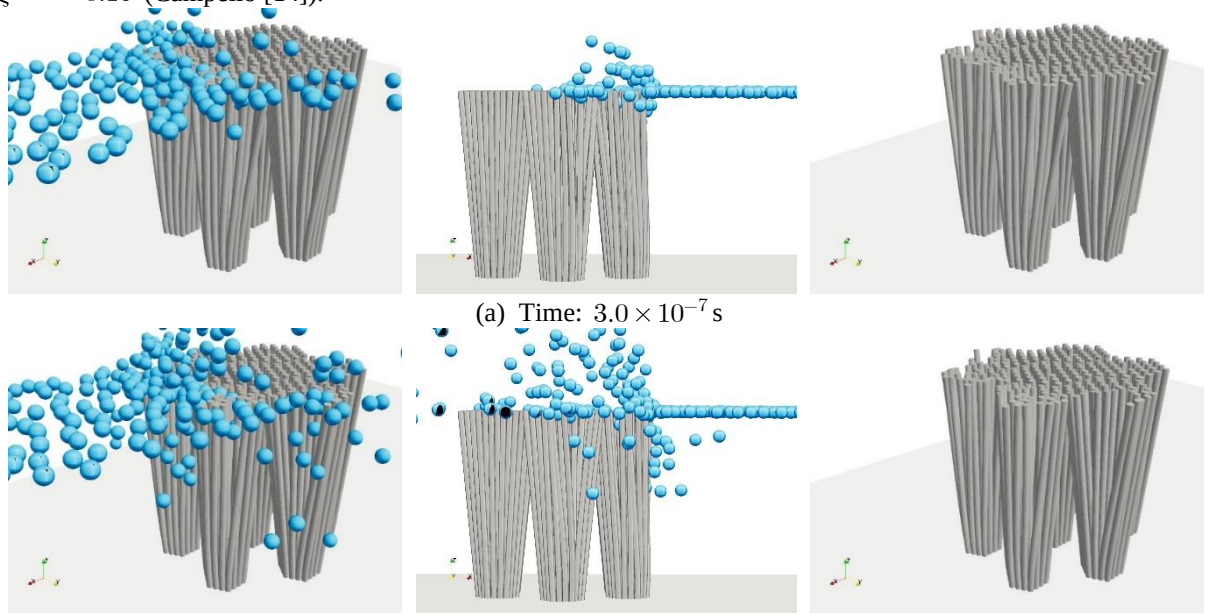

(a) Time: 3.0×10^{-7} s

(b) Time: 6.0×10^{-7} s

Figure 4. Snapshots of of the motion focusing on the EGL deformation through time. The left figure shows the complete system, the midle a side view, and the right one the EGL deformation caused by the particles at the specific time step.

As it can be seen from the snapshots of the simulation in Figs. 3 and 4, as soon as the LDL particles approach the EGL beams, they begin to interact through multipe contacts and collisions, causing the front beams to bend in the direction of the flow and eventually touch other beams that are at the background. The beams, in turn, rebounce some of the LDL particles and also divert the particle flow a bit sideways and in the vertical direction (both up and down) . The interaction is rather complex, and it can be noted that the EGL structure proves to be a rigid physical barrier for the LDL to interact with the endothelial surface.

5 Conclusions

The main purpose of this work was to perform an exploratory investigation of the interaction between LDL particles with the EGL structures that are present in the endothelial surface of the blood vessels. We acknowledge that the problem involves more complex phenomena in addition to the ones herein considered, but at least from a mechanistic point of view, the contact method enforced in our scheme proved to handle properly the motion of both discrete and continuum phases, allowing multiple contacts between each other. The incorporation of more physical phenomena in the model (e.g., adhesion forces) is currently under work.

Acknowledgements. This study was financed in part by the Coordenação de Aperfeiçoamento de Pessoal de Nível Superior – Brasil (CAPES). Second author also acknowledges financial support from CNPq (Conselho Nacional de Desenvolvimento Cientifico e Tecnógico), under the research grant 307368/2018-1.

Authorship statement. The authors hereby confirm that they are the sole liable persons responsible for the authorship of this work, and that all material that has been herein included as part of the present paper is either the property (and authorship) of the authors, or has the permission of the owners to be included here.

References

[1] A. Gay Neto and E. M. B. Campello, "Granular materials interacting with thin flexible rods," *Computational Particle Mechanics,* vol. 4, no. 2, pp. 229-247, 2017.

[2] R. A. Andreotti, E. M. B. Campello and A. Gay Neto, "A two-code coupling strategy for the simulation of particle-structure interaction problems," *Advances in Engineering Software,* (to appear).

[3] X. Liu, Y. Fan and X. Deng, "Effect of the endothelial glycocalyx layer on arterial LDL transport under normal and high pressure," *Journal of Theoretical Biology,* vol. 283, no. 1, pp. 71-81, 2011.

[4] G. Karner, K. Perktold and H. P. Zehentner, "Computational Modeling of Macromolecule Transport in the Arterial Wall," *Computer Methods in Biomechanics and Biomedical Engineering,* vol. 4, no. 6, pp. 491-504, 2001.

[5] L. Ai and K. Vafai, "A coupling model for macromolecule transport in a stenosed arterial wall," *International Journal of Heat and Mass Transfer,* vol. 49, no. 9-10, pp. 1568-1591, 2006.

[6] G. Saidel, E. Morris and G. Chisolm III, "Transport of macromolecules in arterial wall: A mathematical model and analytical solutions," *Bulletin of Mathematical Biology,* vol. 49, no. 2, pp. 153-169, 1987.

[7] P. E. Vincent, S. J. Sherwin and P. D. Weinberg, "The effect of the endothelial glycocalyx layer on concentration polarisation of low density lipoprotein in arteries," *Journal of Theoretical Biology,* vol. 265, no. 1, pp. 1-17, 2010.

[8] A. R. Pries, T. W. Secomb and P. Gaehtgens, "The endothelial surface layer," *Pflügers Archiv - European Journal of Physiology,* vol. 440, no. 5, pp. 653-666, 2000.

[9] S. Weinbaum, J. M. Tarbell and E. R. Damiano, "The Structure and Function of the Endothelial Glycocalyx Layer," *Annual Review of Biomedical Engineering,* vol. 9, no. 1, pp. 121-167, 2007.

[10] Y. Han, S. Weinbaum, J. A. E. Spaan and H. Vink, "Large-deformation analysis of the elastic recoil of fibre layers in a Brinkman medium with application to the endothelial glycocalyx," *Journal of Fluid Mechanics,* vol. 554, no. -1, p. 217, 2006.

[11] P. M. Pimenta and T. Yojo, "Geometrically Exact Analysis of Spatial Frames," *Applied Mechanics Reviews,* vol. 46, no. 11S, pp. S118-S128, 11 1993.

[12] P. M. Pimenta, E. M. B. Campello and P. Wriggers, "An exact conserving algorithm for nonlinear dynamics with rotational DOFs and general hyperelasticity. Part 1: Rods," *Computational Mechanics,* vol. 42, no. 5, pp. 715-732, 10 2008.

[13] P. Wriggers, Nonlinear Finite Element Methods, Berlin, Heidelberg: Springer Berlin Heidelberg, 2008.

[14] E. M. Campello, "A computational model for the simulation of dry granular materials," *International Journal of Non-Linear Mechanics,* vol. 106, no. March, pp. 89-107, november 2018.

[15] E. M. B. Campello, "Um modelo computacional para o estudo de materiais granulares," São Paulo, 2016.

[16] E. M. B. Campello, "A description of rotations for DEM models of particle systems," *Computational Particle Mechanics,* vol. 2, pp. 109-125, 2015.

[17] A. Gay Neto, P. M. Pimenta and P. Wriggers, "A master-surface to master-surface formulation for beam to beam contact. Part I: frictionless interaction," *Computer Methods in Applied Mechanics and Engineering,* vol. 319, pp. 400-429, 5 2016.

[18] E. M. B. Campello, "PSY: particle systems analysis program. User's manual," São Paulo, 2013.

[19] A. Gay Neto, "The giraffe project. User's manual.," 2014.

[20] T. B. Grammer, M. E. Kleber, W. März, G. Silbernagel, R. Siekmeier, H. Wieland, S. Pilz, A. Tomaschitz, W. Koenig and H. Scharnagl, "Low-density lipoprotein particle diameter and mortality: the Ludwigshafen Risk and Cardiovascular Health Study," *European Heart Journal,* vol. 36, no. 1, pp. 31-38, 2015.

[21] S. Takeda, A. Subagyo, S.-P. Hui, H. Fuda, R. Shrestha, K. Sueoka and H. Chiba, "Elastic modulus of low-density lipoprotein as potential indicator of its oxidation," *Annals of Clinical Biochemistry: International Journal of Laboratory Medicine,* vol. 52, no. 6, pp. 647-653, 2015.

[22] M. Klarhöfer, B. Csapo, C. Balassy, . J. C. Szeles and E. Moser, "High-resolution blood flow velocity measurements in the human finger," *Magnetic Resonance in Medicine,* vol. 45, no. 4, pp. 716-719, 2001.

[23] T. Kenner, "The measurement of blood density and its meaning," *Basic Research in Cardiology,* vol. 84, no. 2, pp. 111-124, 1989.

[24] E. Nader, S. Skinner, M. Romana, R. Fort, N. Lemonne, N. Guillot, A. Gauthier, S. Antoine-Jonville, C. Renoux, M.-D. Hardy-Dessources, E. Stauffer, P. Joly, Y. Bertrand and P. Connes, "Blood Rheology: Key Parameters, Impact on Blood Flow, Role in Sickle Cell Disease and Effects of Exercise," *Frontiers in Physiology,* p. 10, 2019.